Thermodynamics and Dynamics for a Model Potential Energy Landscape†

J. Chowdhary‡ and T. Keyes*

Department of Chemistry, Boston University, Boston, Massachusetts 02215

Received: June 2, 2004; In Final Form: August 20, 2004

The local minima or *inherent structures* (IS) and connected first-order saddles (transition states) are obtained with numerical methods for the $N = 32$ unit density Lennard-Jones system. Thermodynamic properties of the normal and supercooled liquid states are calculated with the energy distribution of the IS (density of states (DOS)), and approximations for the harmonic and anharmonic vibrational free energy. Different definitions of the configurational entropy, S_c, are compared and the Adam−Gibbs relation is found to hold using S_c from the IS formalism. The rearrangement pathways between connected neighbor IS are characterized using different measures that are then interpreted with catastrophe theory and the soft potential model. The barrier height distribution is calculated as a function of IS energy, and its relation to the self-diffusion constant, D, and to supercooled dynamics in general, are discussed.

I. Introduction

Glassy materials are ubiquitous in nature and have a wide range of technological applications. Understanding their formation and properties is therefore of particular interest. Traditionally, glasses are formed by starting with a hot liquid and rapidly cooling it until dynamical arrest sets in and the system shows solidlike properties. A number of dramatic changes in the dynamic and thermodynamic properties occur[1] during this process, e.g., apparent divergence of the viscosity and a jump in the constant pressure heat capacity in the vicinity of the glass transition temperature T_g, which is conventionally defined via the shear viscosity η, $\eta(T_g) = 10^{13}$ poise.

Liquids are classified[1] as strong or fragile according to the T dependence of η; the self-diffusion constant, D, also serves if the Stokes−Einstein law holds, $D \propto T/\eta$. The slope of a plot of $\log(\eta(T))$ vs $1/T$ defines an activation energy $E_A(T)$. For strong liquids (e.g., SiO_2), E_A is a constant. Fragile liquids (e.g., ortho-terphenyl) exhibit "super-Arrhenius" behavior: $E_A(T)$ is small at room temperature but escalates dramatically with cooling. The increase begins near the[2] mode coupling temperature, T_c, where D has decreased by 3−4 decades and extrapolates to zero from above, and molecular dynamics simulation becomes problematic.

In the extended classification of Kivelson and co-workers,[3] substances are fragile or nonfragile depending on whether they have super-Arrhenius or Arrhenius T dependence at low T, respectively. Additionally, the high-T behavior determines whether a substance is weak or strong, for $E_A \leq T$ and $E_A \gg T$, respectively.

Although a number of phenomenological models, such as the Adam−Gibbs model,[4] and approximate theories such as mode coupling[2] and fluctuation-limited domain theory[5] exist, a complete understanding of glassy phenomenology is still unavailable. A fruitful approach toward understanding supercooled liquids was proposed by Goldstein[6] in a remarkably prescient paper where he formulated dynamics in terms of the $3N$-dimensional *potential energy landscape* (PEL), the topology of the potential energy, $U(\boldsymbol{r})$, as a function of all the atomic coordinates, denoted $\boldsymbol{r}$, of an N-atom system. At low T the waiting time of the system the basin associated with a local minimum is much longer than the vibrational time. Relaxation requires visiting a transition state, a first-order saddle, and thence an adjoining basins. Thus liquid-state dynamics is formulated as chemical kinetics. At high T the motion of the system is freer. A crossover temperature is associated with the change is dynamical mechanism.

The development of the PEL point of view required new theory and more powerful computers, and has largely been carried out[7] by Stillinger and co-workers. Stillinger and Weber[8,9] formulated an exact thermodynamic theory based on partitioning the PEL into basins of attraction of the local minima, which they named *inherent structures* (IS); each liquid configuration is mapped to an IS via steepest descent minimization. We will utilize the canonical ensemble. All quantities depend on both density and temperature, but the density dependence will be left implicit. The partition function can then be rewritten in terms of the energy distribution of IS, $\Omega(U_{is})$, called the density of states (DOS) in the following, where U_{is} is the IS energy, and the vibrational Helmholtz free energy, $A_{vib}(U_{is},T)$, determined by the configurational integral for a system confined to a basin. With these quantities and their density dependence, the thermodynamic Helmholtz free energy, $A(T)$, and the equation of state[10−13] can be evaluated.

Dynamics may be regarded[8] as motion among the IS "states". With information about the connected IS and IS transitions, the self-diffusion constant, D,[14] and the change in mechanism of diffusion with decreasing T[15] can be studied. This formalism is especially suitable for supercooled liquids. An alternative approach[16] is to use all the stationary points, including both saddles and minima, as states.

A general statement of the PEL hypothesis for dynamics is: *The properties and arrangement of the stationary points determine the interesting features of supercooled dynamics*.

Related approaches are trap,[18] random barrier,[19] and random energy models.[22,23] In trap models the top of the landscape is assumed to be flat with the system spending long times in deep traps, which can be identified either as IS or groups of IS, the so-called metabasins. Assuming a particular distribution for trap

† Part of the special issue "Frank H. Stillinger Festschrift".

‡ Present address: Chemistry Department, Colorado State University, Fort Collins, Colorado 80523.

10.1021/jp047615t CCC: $27.50
Published on Web 10/26/2004

depths (E_t) and a rate of escape, $\exp(-E_t/T)$, glassy dynamics can be modeled. The random barrier model assumes hopping between sites over barriers selected from a distribution irrespective of the site. Exact results can be obtained in all dimensions for trap models, but only in one dimension for random barrier models. Neither predicts Arrhenius T dependence for D, which is observed in strong network forming liquids. Limoge and Bocquet[20] suggested that a combination of random trap and random barrier models could give Arrhenius behavior and such is indeed the case.[21] A third approach,[22,23] the random energy model, builds up the landscape from the properties of local regions and has been applied to supercooled liquids and proteins. A prerequisite for all these models is the distribution of trap energies or barrier heights or connected states that are usually not known a priori but can be inferred indirectly.

For typical simulations with hundreds to thousands of particles, complete information of the landscape is unavailable due to computational limitations. The number of distinct IS increases exponentially[17] and obtaining a complete database of IS and transition states is not feasible. It then makes sense to study systems that are small enough for a database to be constructed but large enough to exhibit at least qualitative features of supercooled liquids. There is an extensive literature on finite size clusters, obtaining complete catalogs of IS and transition states,[24] and their connection to cluster thermodynamics.[25] Dynamics can then be modeled in terms of the master equation[26] and typical features of low-T systems such as nonexponential relaxation have been demonstrated.[27]

In previous work[14,15] we have studied diffusion and its mechanism in the IS formalism for an $N = 32$ unit density Lennard-Jones (LJ) system using molecular dynamics (MD) simulations. According to Kivelson et al.[3], unit-density LJ is a weak, nonfragile liquid, possibly the most nonfragile known liquid, with T_g close to zero K.

Here we construct an exhaustive catalog of the IS and transition states for the same system, relate them to thermodynamics and dynamics, and make comparisons with simulation. In part II, we describe the simulation technique. Part III concerns thermodynamics. We present the DOS, and the harmonic approximation to the vibrational free energy and its IS energy dependence. Because the system is anharmonic in general, we propose an alternative to basin constrained simulations for obtaining anharmonicity corrections. With the DOS and A_{vib} available, we go on to calculate the average IS energy, $U_{is}(T)$, and compare it with simulation data.

The configurational entropy, $S_c(T)$, plays an important role in the thermodynamics of supercooled liquids. Experimentally it is the difference in entropy of the liquid and the crystal at constant temperature and pressure. An alternative, natural definition in the IS formalism is the difference in the total entropy and vibrational entropy of the liquid. The configurational entropy extrapolates to zero at the Kauzmann temperature, $T_K > 0$, and apparently possesses negative values below T_K, the so-called Kauzmann paradox. We calculate the entropy and free energy of the liquid and the fcc crystal with thermodynamic integration, calculate $S_c(T)$ with both definitions and compare the results. Because the simulations are carried out at constant density the quantity obtained is $S_c(T,\rho)$, not the usual $S_c(T,P)$. The constant pressure and constant density values of T_K are of course not expected to be the same. Finally, we estimate the DOS from the IS sampled at a given T, invoking the anharmonic vibrational free energy, and compare it with the complete DOS

Next we address dynamics. Understanding diffusion requires information about its elementary steps, the multiparticle rearrangement pathways (RP), and their relation to D. In an activated barrier crossing picture of low-T dynamics on the PEL, the elementary step for diffusion involves going from an IS over a connected transition state to a new IS. In an entropic transport picture, barriers are irrelevant and it is the connectivity among the IS that governs the dynamic slowing down in supercooled liquids.

In section IV, we characterize the RP in terms of the inter-IS distance, the path length going from an IS to a connected transition state, the number of atoms involved in the rearrangement, the barrier height distribution and correlations with the eigenfrequency at the transition state. The RP are then modeled with the soft potential model,[28,29] which has been used in studies of thermodynamics of deeply supercooled liquids. The soft modes are either single wells, or symmetric or asymmetric double wells depending on the potential parameters. We summarize the information on the RP in terms of the distribution of the parameters and their implications for the glass transition temperature are discussed. In addition, the form of the RP in parameter space is interpreted with catastrophe theory.[30,31]

In section V, dynamics is described in terms of the RP and the barrier height distributions. Possible relations between D and the average rate or average inverse rate for crossing a barrier are proposed. The IS−energy dependent barrier height distribution, $\Gamma(B;U_{is})$, is presented. A calculation of the averaged rate reproduces the simulated T dependence of D. The relative contribution of small and large energy barriers to the diffusion constant in terms of a rate is quantified, with the conclusion that barriers smaller than k_bT are dominant, i.e., "entropic transport".

II. Simulation Detals

MD simulations are carried out for a unit-density $N = 32$ supercooled LJ system. The details are presented in ref 14 and briefly summarized here. Natural LJ units will be used for numerical calculations, results and figures throughout the paper. A hot liquid at $T = 5.0$ is cooled in one step to $T = 1.2$, and the temperature lowered further in steps of 0.02 until $T = 0.4$. For each T, the system is equilibrated for $2.5\tau_{LJ}$ and data collected for $62.5\tau_{LJ}$ corresponding to a cooling rate of 3.08×10^{-4}. This is repeated 40 times to generate an ensemble of quenches. A run is terminated when and if the pair distribution becomes solidlike. Conjugate-gradient minimizations[32] are performed every 200 time steps ($dt = 0.00125$) with the instantaneous and IS configurations saved for further analysis.

With the IS configurations from the simulations, an initial database is compiled such that the energy difference between any two IS is at least 1.0×10^{-6}, as a first attempt to avoid overcounting. Then, the Hessian is constructed for each IS and its eigenanalysis carried out. Eigenvector-following calculations are initiated along modes with the 32 lowest nonzero eigenvalues to obtain the transition states. Next, for all the saddles, the configuration is displaced along and opposite to the eigenvector corresponding to the negative eigenvalue with a steplength of 0.01 and steepest descent minimization initiated using the Burlisch−Stoer method.[32] The final configurations are verified to be local minima on the basis of the number of negative and zero eigenvalues, saved, and the transition state calculations are repeated with all the new IS until no new IS are found. In all 18 000 distinct saddles and 10 000 local minima, excluding those connected to the crystal, were obtained

There is no guarantee that the catalog so compiled is complete. As a test of convergence, starting from the crystal, the configuration is perturbed along random directions by

random distances and the resulting configurations minimized. Few new IS were obtained with 100 000 minimizations, and they had high energies and are not expected to contribute to supercooled liquid properties.

Further MD simulations were carried out to obtain the density dependence of the excess pressure, over the ideal gas, for $T = 5.0$ and $0.001 \leq \rho \leq 1.0$. For unit density, the temperature dependence of the potential energy from $T = 5.0$ to $T = 1.2$ was determined to supplement the data from the cooling runs described earlier. Starting with a $T = 5.0$ ideal gas state, thermodynamic integration was then carried out to calculate the T-dependent free energy and entropy. For obtaining the entropy of the crystalline state as a function of T, the fcc lattice was heated in a stepwise manner from $T = 0.1$ to $T = 2.0$ and the melting temperature was found to be $T \approx 1.6$.

III. Thermodynamics in the Inherent Structure Formalism

The ingredients of Stillinger's[7] IS formalism are the DOS, $\Omega(U_{is})$, and the vibrational free energy, $A_{vib}(U_{is},T)$, which yield the partition function,

$$Q(T) = \int \mathrm{d}U_{is}\, \Omega(U_{is}) \mathrm{e}^{-(U_{is}+A_{vib}(U_{is},T))/k_BT} \tag{1}$$

with A_{vib} defined as

$$\exp(-A_{vib}(U_{is},T)/k_BT) = \frac{1}{\Lambda^{3N}} \frac{\sum' \int_{V\,\mathrm{basin}} \mathrm{d}\mathbf{r}\, \exp(-(U(\mathbf{r}) - U_{is})/k_BT)}{\Omega(U_{is})\Delta U_{is}} \tag{2}$$

where the prime indicates a sum over all IS with energy in the range U_{is} and $U_{is} + \Delta U_{is}$, Λ is the de Broglie wavelength, and the integral is over the volume of the basin. The contributions of the momenta are incorporated into A_{vib}. Boltzmann's constant, k_B, does not appear explicitly after changing to LJ units.

In a simulation at a given T, one can determine the average IS energy, $U_{is}(T)$ and the distribution of IS energies, $P(U_{is},T)$, which obey

$$P(U_{is},T) = \frac{\Omega(U_{is}) \exp(-(U_{is} + A_{vib}(U_{is},T))/k_BT)}{Q(T)} \tag{3}$$

and $U_{is}(T) = \int \mathrm{d}U_{is}\, U_{is}P(U_{is},T)$. We write $U_{is}(T)$ instead of $\langle U_{is}(T)\rangle$ to simplify the notation for an average at fixed T when the meaning is transparent.

A configurational entropy may be estimated from the number of available IS by Boltzmann's formula, $S_c(U_{is}) = k_B \ln(\Omega(U_{is})\Delta)$, where Δ has units of energy but otherwise does not influence the calculation. The corresponding T-dependent quantity is $S_c(T) = \int \mathrm{d}U_{is}\, S_c(U_{is})P(U_{is},T)$. It is usually easier to subtract the vibrational contribution, S_{vib}, from the total entropy, $S(T)$, of the liquid. The vibrational contribution may be divided into a harmonic $S_{harm}(T)$ and an anharmonic $S_{anh}(T)$,

$$S_c(T) = S(T) - S_{harm}(T) - S_{anh}(T) \tag{4}$$

In experiments, S_c is typically calculated by subtracting the entropy of the crystal (xtl) from that of the liquid. The vibrational contributions of the liquid and crystal entropy are assumed to be similar. Then

$$S_c^E(T) = S(T) - S_{xtl}(T) \tag{5}$$

We will compare the two definitions in the following.

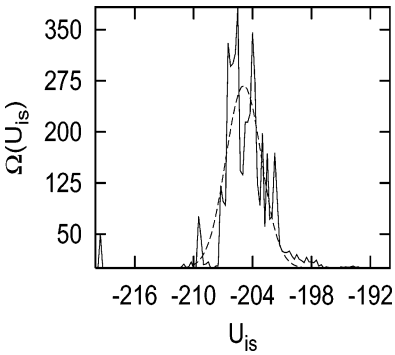

Figure 1. Inherent structure density of states for $N = 32$ unit density LJ and Gaussian fit. The peak at $U_{is} = -219.5$ corresponding to the crystal has been exagerated.

A. Inherent Structure Density of States. Figure 1 shows the DOS obtained from the eigenvector following and perturbed-crystal minimization database. The fcc lattice is the global minimum for this system and is separated from the other minima by an energy gap. The significant liquidlike DOS for low-T simulation consists of a narrow low-energy band and a broader, higher energy band. There is a narrow high-energy band, centered around $U_{is} = -192.0$, that exists but is never sampled except possibly at extremely high T (not shown in Figure 1).

For a landscape composed of independent cooperatively rearranging regions, the DOS can be shown to be a Gaussian in the large-N limit.[22,23] The deviations just discussed are indicative of finite size effects. Nevertheless, a single Gaussian is a reasonable and conceptually significant representation,

$$\Omega(U_{is}) = \exp\left(\alpha N - \frac{(U_{is} - U_0)^2}{2\sigma^2}\right) \tag{6}$$

where $U_0 = -204.905$, $\sigma^2 = 3.241$, and $\alpha = 0.29$.

B. Vibrational Free Energy. The second component of IS thermodynamics is the vibrational free energy, defined in eq 2. Below T_c it is plausible that the system is usually close to the bottom of the basin, where a Taylor expansion of U up to second order is sufficient. The harmonic approximation for a specific IS results,

$$A_{harm}/k_BT = \sum_i^M \ln(\hbar\omega_i/k_BT) \tag{7}$$

which can be rewritten to separate out the U_{is} dependent and T dependent parts as

$$A_{harm}/k_BT = M \ln(\hbar\omega_0/k_BT) + \sum_i^M \ln(\omega_i/\omega_0) \tag{8}$$

where ω_i is the ith normal-mode frequency for the selected IS, $M = 3N - 3$ and $\omega_0 = 1/\tau_{LJ}$.

Defining $H = \sum_i^M \ln(\omega_i/\omega_0)$, the U_{is} dependence is shown in Figure 2 as a scatter plot. The overall trend is that IS with higher U_{is} have larger H. However, one can identify distinct U_{is} dependences in three regions, $U_{is} < -209$, $-209 < U_{is} < -197$, and $U_{is} > -197$.

Though the scatter plot is informative, the quantity that enters the partition function following the cummulant approximation, $\langle A_{vib}\rangle(U_{is})$, contains the average of the frequency sum over all IS in a given energy band, denoted $H(U_{is})$, and is shown in Figure 3. An almost quadratic U_{is} dependence is found for the entire range of liquidlike IS. A more detailed representation

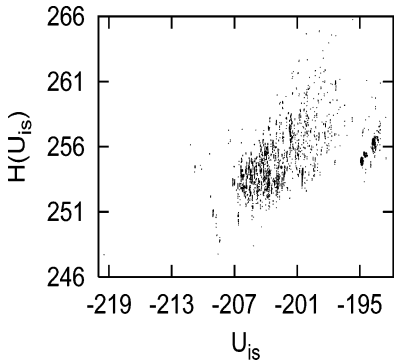

Figure 2. Inherent structure energy dependence of the sum $H = \sum_{i=1}^{3N-3} \ln(\omega_i/\omega_0)$ for all IS in the database.

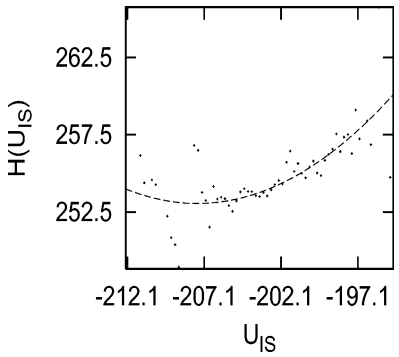

Figure 3. Inherent structure energy dependence of the average $H(U_{is})$. The smooth curve is a quadratic fit to the data.

TABLE 1: Coefficients for the Anharmonic Free Energy for the Liquid-Like Inherent Structures and the Crystal

k	a_k	b_k	c_k
1	2120.64	−981.014	24.0131
2	17.9966	−9.9277	−11.6094
3	0.0434	−0.02501	2.4526

would involve a linear dependence for $U_{is} < -209$ and a quadratic dependence for $-209 < U_{is} < -197$. For the sake of simplicity we select a single quadratic function,

$$H(U_{is}) = a_1 + a_2 U_{is} + a_3 U_{is}^2 \tag{9}$$

and the coefficients are summarized in Table 1.

For $T > T_c$, the system starts exploring the PEL and sees the finite size of the basin of attraction of the IS, and anharmonicities become important. The vibrational free energy can then be written as a sum of harmonic and anharmonic contributions, $A_{vib} = A_{harm} + A_{anh}$. In previous work on IS thermodynamics, anharmonicities have been treated as U_{is} independent,[33−35] or the U_{is} dependence was obtained using basin constrained simulations.[36] The latter is not computationally feasible for all the IS in the database, and an alternative method is needed to obtain the energy dependence of the anharmonic free energy.

For a given basin, anharmonicity corrections can be systematically included in the framework of perturbation theory.[37,38] The corrections are expressed as an infinite series in T, with the coefficients related to higher order (>2) derivatives of the average $U(T)$.

For large systems, the exponential increase in the number of distinct IS, the increasing computational cost in evaluating higher order derivatives, and effect of truncation renders a series expansion infeasible. Lacks and Shukla[39] proposed an alternative technique involving a basin constrained MD simulation. The deviation of the potential energy from the harmonic approximation is utilized for estimating A_{anh} as a function of both T and U_{is}, the IS energy to which the system is constrained,

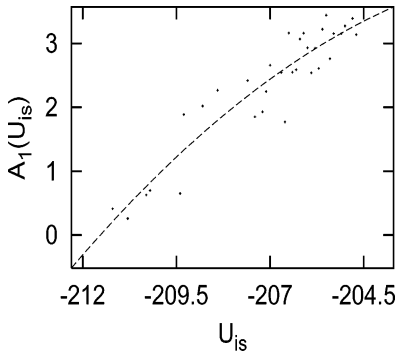

Figure 4. Inherent structure energy dependence of the anharmonic free energy correction term, $A_1(U_{is})$. The smooth curve is a quadratic fit to the data.

$$A_{anh}(U_{is},T)/k_B T = \sum_{n=1} A_n(U_{is}) T^n \tag{10}$$

from which one can obtain the anharmonic energy,

$$U_{anh}(U_{is},T) \equiv U(U_{is},T) - U_{is} - 1.5(N-1)k_B T = \sum_{n=1} (-nA_n(U_{is}))T^{n+1} \tag{11}$$

An attempt to evaluate the coefficients, $A_n(U_{is})$, with extensive basin-constrained simulation would still be computationally inconvenient; thus we employ an alternative method. Starting with a database of instantaneous energies and the corresponding IS energies from finite-T MD runs, one can collect the conditional average potential energy, $U(U_{is},T)$, when the system maps to an IS with energy in the range (U_{is}, $U_{is} + \Delta U_{is}$). The average potential energy, $U(T)$, is the average of $U(U_{is},T)$ over all IS energies sampled at T. Then the anharmonic energy for each IS energy band can be fit using eq 11. The coefficients $A_n(U_{is})$ so obtained are representative of that IS energy band unlike in eq 11 where they represent individual IS, but we retain the same notation.

Because not all IS energies are sampled at each T and binning the instantaneous energies increases the noise in $U(U_{is},T)$, as compared to $U(T)$, we select only those bands that are sampled for at least 30 temperatures in our cooling runs. To obtain the leading anharmonicity correction to A_{vib}, we retain the $n = 1$ term in eq 11 and fit the T dependence of the anharmonic energy to

$$U_{anh}(U_{is},T) = (-A_1(U_{is}))T^2 \tag{12}$$

The U_{is} dependence of A_1 is shown in Figure 4 and is fit to a quadratic in U_{is},

$$A_1(U_{is}) = b_1 + b_2 U_{is} + b_3 U_{is}^2 \tag{13}$$

The parameters are summarized in Table 1.

Finally, recognizing that the crystal is anharmonic except at the lowest T, we obtain corrections for anharmonicty using the premelting part of a melting run, which is essentially a basin constrained simulation for the crystalline minimum. Truncating eq 11 at $n = 3$ and fitting the anharmonic energy in the crystal, we obtain

$$A_{anh}^{xtl}/k_B T = c_1 T + c_2 T^2 + c_3 T^3 \tag{14}$$

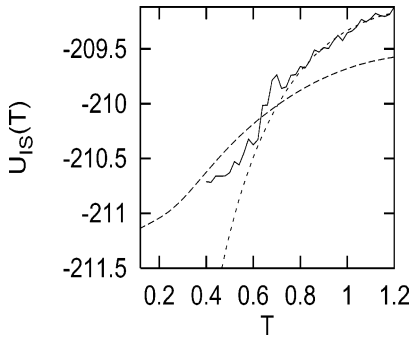

Figure 5. Temperature dependence of the average IS energy. The curves from bottom to top at $T = 0.5$ are analytical anharmonic expression, simulation data, and exact DOS and harmonic free energy.

The parameters are in Table 1. With the DOS and an approximate A_{vib}, different thermodynamic averages can be evaluated and compared with simulation.

C. Average Inherent Structure Energy. One of the simplest PEL quantities to calculate in simulations is the average IS energy, $U_{is}(T)$. Using a Gaussian approximation (eq 6) for the DOS and quadratic U_{is} dependence for $H(U_{is})$ (eq 9) and the anharmonic free energy (eq 13), the integrand of eq 1 has its maximum at

$$U_{is}(T) = \frac{U_0 - \sigma^2\left(\frac{1}{T} + a_2 + b_2 T\right)}{1 + 2\sigma^2(a_3 + b_3 T)} \tag{15}$$

We fit the high-T part of the simulated $U_{is}(T)$ to eq 15 using U_0 and σ^2 as the variables and obtain (LJ units) values of $U_0 = -205.104$ and $\sigma^2 = 3.015$, which are in excellent agreement with values from the Gaussian fit to the DOS of $U_0 = -204.905$ and $\sigma^2 = 3.241$. The resulting $U_{is}(T)$ is plotted in Figure 5, and it reproduces the simulation results for $T > 0.6$ including the high-T plateau typically found in LJ-like systems. This represents a significant improvement over the Gaussian harmonic approximation used in previous works.[34] The low-T plateau is not reproduced. This is expected because, unlike the true DOS, the Gaussian does not have a lower cutoff.

To ascertain the importance of anharmonicity, we calculate a "best" harmonic approximation to $U_{is}(T)$ by taking the average with eq 3, using the full DOS—literally summing over all the IS in the database—and the exact values of H for each individual IS. The result (Figure 5) is shifted to lower energies, as is expected because the structure in the true DOS causes its mean to differ from that of the Gaussian approximation. Like the DOS, it shows a low-T plateau, but the temperature at which the plateau is reached and its energy are much lower than the value from simulations. The "best harmonic" approximation, even using the true DOS, is inferior to our approximate anharmonic theory.

In addition to our approximations, the $U_{is}(T)$ calculation represents a restricted equilibrium average (excluding the crystal), which would correspond to infinitely slow cooling whereas the simulation results are for a finite cooling rate. It is known that the low-T plateau in $U_{is}(T)$, as observed in a binary-LJ mixture,[40] is a function of the cooling rate with the plateau temperature decreasing with slower cooling. The high-T plateau and the early stages of the fall off from the high-T plateau are fairly cooling rate independent and it is in this regime that the analytical anharmonic calculation is consistent with simulation.

D. Configurational Entropy. The total entropy is usually calculated using thermodynamic integration.[35] Starting with the entropy and free energy of the ideal gas at a reference high temperature, $T_R = 5.0$, and carrying out an isothermal integration up to unit density, followed by an isochoric integration from T_R to the state point of interest, the entropy of the liquid, $S(T)$, and its free energy, $A(T)$, can be obtained. In terms of eq 4, the configurational entropy can be obtained by subtracting the vibrational entropy, S_{vib}, from the total entropy. The harmonic contributions to S_{vib} is

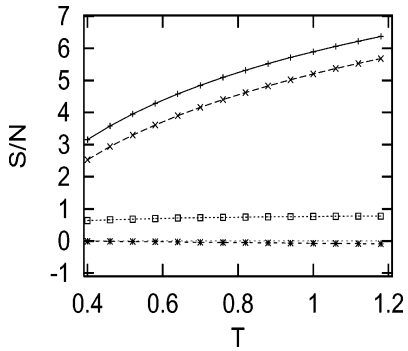

Figure 6. Temperature dependence of entropy and its components. Top to bottom: $S(T)$, $S_{harm}(T)$, $S_c(T)$, and $S_{anh}(T)$.

$$S_{harm}(T)/k_B = (3N - 3)[1 - \ln(\hbar\omega_0/k_B T)] - \langle H(T)\rangle \tag{16}$$

whereas the anharmonic contribution can be obtained using the anharmonic energy as obtained in section III.B.

$$S_{anh}(T,U_{is}) = \int \frac{dT}{T}\frac{dU_{anh}(T,U_{is})}{dT} \tag{17}$$

Using eqs 12 and 13 and averaging over all IS accessed at the given T, one can rewrite eq 17 as

$$S_{anh}(T) = -2T(b_1 + b_2 U_{is}(T) + b_3\langle U_{is}{}^2(T)\rangle) \tag{18}$$

The results are shown in Figure 6. The prominent contribution to $S(T)$ comes from the harmonic entropy whereas $S_{anh}(T)$ takes on increasingly negative values with increasing T. The negative anharmonic entropy is indicative of the finite size of the basin, which is not accounted for in the harmonic approximation, leading to a too-large configurational space volume. In a sense the system is quite harmonic but note that S_{anh} is the anharmonic *vibrational* entropy; the configurational entropy, related to the liquidlike properties, is entirely anharmonic. $S_c(T)$ extrapolates to zero at the Kauzmann temperature, T_K, below which it is negative. Using a power law fit over the entire T range gives $T_K = 0.155$, whereas the value estimated from the diffusion constant data using the Vogel—Fulcher—Tamman equation is 0.003. A fit using a fifth-order polynommial, however, gives $T_K = 0.065$. The dependence of the Kauzmann temperature on the fitting function has been emphasized in the context of resolving the Kauzmann paradox by Johari.[41]

The configurational entropy can also be obtained using eq 5, where it is assumed the vibrational contribution to the liquid and crystal entropies are similar. In the IS formalism the only contribution to the crystal entropy is vibrational, S_{vib}^{xtl}. The difference between the two possible definitions of configurational entropy, $dS_c(T) = S_c^E(T) - S_c$, can be written in terms of the difference in the vibrational contribution to the liquid and crystal entropies, $dS_c(T) = S_{vib}(T) - S_{vib}^{xtl}(T)$, which in general is nonzero. For this system, $S_c(T)$ and S_c^E can be calculated using eqs 9, 13, and 14 and $H(U_{is})$ for the crystal and is shown in Figure 7. Clearly $S_c^E(T)$ has a larger magnitude than $S_c(T)$

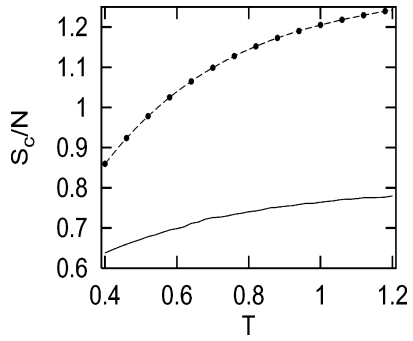

Figure 7. Temperature dependence of configurational entropy of the liquid calculated as the difference in the total and vibrational entropies (S_c, bottom) and as the difference in liquid and crystal entropies (S_c^E, top, solid circles). The smooth curve on the top is S_c plus the difference in vibrational entropies of the liquid and crystal.

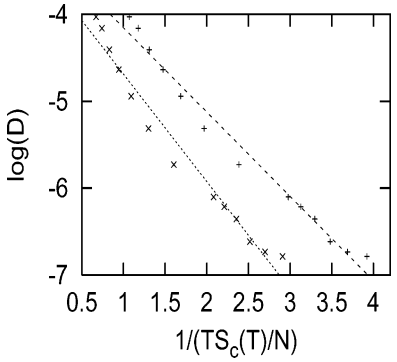

Figure 8. Test of the Adam−Gibbs relation $\ln(D) \propto (1/(TS_c(T)))$: upper curve, with S_c; lower curve, with S_c^E.

and a power law extrapolation to zero gives $T_K^E = 0.27$, which is larger than T_K estimated from $S_c(T)$. The difference can be accounted for (Figure 7) by including the difference in vibrational entropies $dS_c(T)$ and needs to be considered in interpreting experimental configurational entropies.

Adam and Gibbs[4] proposed a connection between configurational entropy and relaxation times. Figure 8 demonstrates that the Adam−Gibbs relation, $\ln(D) \propto (1/TS_c(T))$, is well obeyed for both definitions of configurational entropy. This is so despite the insufficient removal of the vibrational entropy from S_c^E, and despite our application of the relation at constant density instead of constant pressure.

E. Density of States Derived from Simulation. It is desirable to obtain the DOS, which is equivalent to $S_c(U_{is})$, without brute-force enumeration of all the IS; this requires a good theory of A_{vib}, including anharmonicity. Taking the natural log of eq 3, writing $\ln(Q(T))$ in terms of the total Helmholtz free energy $A(T)$, and inserting the expression for A_{vib}, we have

$$S_c(U_{is}) = U_{is}/T + k_B M \ln(\hbar\omega_0/k_B T) + \sum_1^3 (k_B a_i + b_i T) U_{is}^{i-1} - A(T)/T + k_B \ln(P(U_{is},T)) \quad (19)$$

Because $P(U_{is},T)$ is readily available from simulation, $A(T)$ can be calculated from thermodynamic integration and the remaining terms correspond to the vibrational free energy, the right-hand side of eq 19 can be calculated. We select a high enough temperature, $T = 1.20$, so that a broad range of U_{is} is accessed and estimate $S_c(U_{is})$. Shown in Figure 9 is the $S_c(U_{is})$ obtained from simulations. Because the true DOS was approximated as

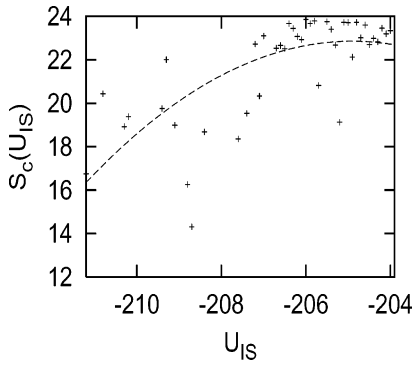

Figure 9. Estimating the configurational entropy for inherent structures from the distribution of IS sampled at $T = 1.20$. The smooth curve is the best quadratic fit to the data.

a Gaussian (eq 6), we fit the $S_c(U_{is})$ so obtained to

$$S_c(U_{is}) = \alpha' N - \frac{(U_{is} - U_0')^2}{2\sigma'^2} \quad (20)$$

and obtain $\alpha' = 0.71$, $U_0' = -204.9$, and $\sigma'^2 = 3.05$. The fit parameters are fairly independent of the temperature from which the data were analyzed.

The value of α' is much larger than the corresponding value from the database. This difference could either be due to the incompleteness of the database or need for a better approximation for A_{vib}. The values for the mean and variance of the distribution are comparable to the values from the database. Clearly with an appropriate vibrational free energy and thermodynamic integration, the DOS can be approximately obtained as in previous works.[42]

IV. Characterizing the Rearrangement Pathways

In the Stillinger−Weber[8] picture of transport in liquids, the unit diffusive step involves the system going from one IS to another via a transition state. These *triplets* of IS−transition state−IS correspond to the zero-temperature rearrangement pathways. All information about the RP are engraved on the PEL and need to be quantified to understand the nature of the diffusive step. The two barrier heights, B, are of primary importance.

One of the simplest features of a RP is the distance between the connected IS in Cartesian space. For a given pair of IS configurations R_1 and R_2 the Cartesian distance is $r_{is1,is2} = |R_1 - R_2|$. This is an important quantity because its thermal average corresponds to a length scale for diffusion.[14] Some of the other easily calculable distances are those between a transition state and the two connected IS, $r_{is,b}$. Given $r_{is1,is2}$ and $r_{is,b}$, one can calculate the number of atoms involved in going from one IS to another ($n_{is1,is2}$) and in going from an IS to the barrier ($n_{is,b}$) by using the participation ratio.

Another distance that is more closely related to the overall rearrangement is the path or contour length ($s_{is,b}$), the sum of all the small displacements along the steepest descent pathway leading from the saddle to the IS. Also significant is the curvature at the barrier, expressed in terms of the single negative eigenvalue (squared imaginary frequency) of the Hessian.

All these quantities can be calculated by displacing the system from the saddle both along and opposite to the negative eigenvector direction at the saddle, obtaining the triplet and analyzing the three configurations. Due to the multiplicity of RP, their properties are best described in terms of distribution functions and correlations. Simulation studies have revealed[40]

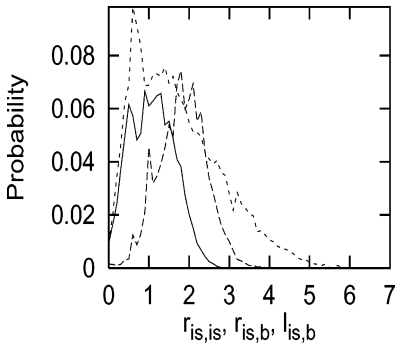

Figure 10. Distribution of IS−IS distance ($r_{is,is}$, large dashes), IS−saddle distance ($r_{is,b}$, smooth line), and path length from saddle to IS ($s_{is,b}$, small dashes).

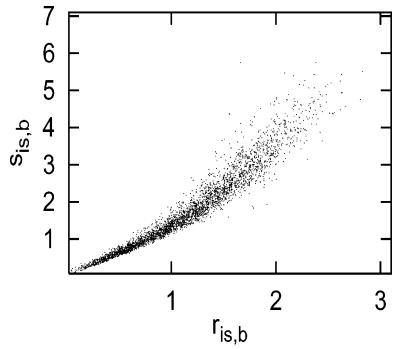

Figure 11. Dependence of the integrated path length, $s_{is,b}$, on the IS−barrier distance in Cartesian coordinates.

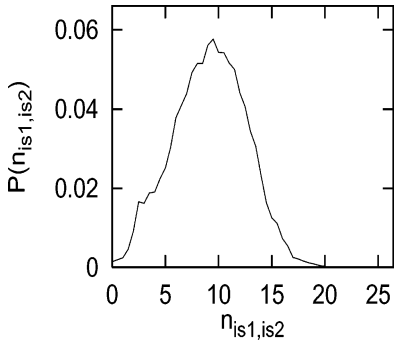

Figure 12. Distribution of the number of atoms involved in an IS transition as obtained from the participation ratio.

that at the temperatures where supercooled liquids exhibit their interesting phenomenology, $U_{is}(T)$ is falling with decreasing T. We seek to understand the T dependence of supercooled dynamics via the U_{is} dependence of the RP.

It is desirable to represent the RP with physically meaningful, analytic one-dimensional functions. One such representation is a quartic "soft potential",

$$V_{spm}(x) = V_s + W(x^4 + d_2x^2 + d_1x) \qquad (21)$$

frequently invoked[28,29] in supercooled and glassy physics. By varying the parameters, $V(x)$ can be a single well, or a symmetric or asymmetric double well potential. These profiles have been used[29,43] to characterize the[44,.45] instantaneous normal modes (INM) of liquidlike configurations, and thence related to diffusion.

The dependence of a function on its parameters, ($d1$,$d2$) in this case, is often described in terms of catastrophe theory[30] and the quartic polynomial is associated with a cusp catastrophe. The set of points ($d1$,$d2$) that characterizes the nonstationary points partition parameter space into open intervals where the function is qualitatively similar. The seperatrix in parameter space consists of the point (0,0) and a "fold curve" inside which $V(x)$ has three nondegenerate roots and outside which $V(x)$ has one minimum. It is significant that the region in parameter space corresponding to three nondegenerate roots corresponds to double well modes which are related to diffusion. With a model for the RP, a relation between the curvature, IS−transition state distance and barrier height can be obtained.[31]

A. Length Scales. The distributions of $r_{is1,is2}$ and $r_{is,b}$ are shown in Figure 10. Both are approximately Gaussian. In previous work[14] it was found that the distribution of IS−transition distances sampled during finite T simulations was bimodal, with an additional, nondiffusive small distance peak. Although the distribution of $r_{is1,is2}$ and $r_{is,b}$ shows no structure, finite T sampling selects a bimodal distribution. A second difference between the distribution from simulation and the RP database is the magnitude of the $r_{is1,is2}$, which extends to large values for the database. This difference is expected if at finite T the system preferentially accesses the closest connected IS. Another feature is that the distribution for $r_{is1,is2}$ is shifted to larger values than that for $r_{is,b}$ by apparently a constant value, suggesting that moving to the saddle and then to the second IS represent two independent steps so far as distance traveled is concerned.

The distribution of $s_{is,b}$ is shown in Figure 10 and appears to be shifted to larger values because $s_{is,b} > r_{is,b}$ in general. It is interesting to note that the distributions for $r_{is1,is2}$ and $s_{is,b}$ are comparable, in both shape and in the magnitudes of the distances occurring, to the corresponding distributions for an $N = 55$ LJ cluster.[24] System-size independence of these pathways might be expected if they are properties of the local regions.

To identify any relation between $r_{is,b}$ and $s_{is,b}$, we make a scatter plot, Figure 11. Two approximately linear regimes can be identified such that $s_{is,b} = mr_{is,b} + p$, where $(m, p) = (1.4, 0.0)$ for $r_{is,b} < 1.2$ and $(m, p) = (2.4, -1.16)$ for $r_{is,b} > 1.2$. Clearly a large $r_{is,b}$ corresponds to a large $s_{is,b}$. It remains to be seen if this linear relation holds in other systems. Outside of the two linear regimes, $r_{is,b}$ and $s_{is,b}$ would appear to be less correlated and there is better correlation for small $r_{is,b}$.

Information about inter-IS distances can be utilized to estimate a participation ratio,[8] which can be interpreted as the number of atoms, $n_{is1,is2}$, involved in a transition. The distribution, shown in Figure 12, is broad and peaked at about $n_{is1,is2} = 9$, with a shoulder at $n_{is1,is2} = 3$. In previous work on the same system[14] we found $n_{is1,is2} \approx 7$, just a bit smaller than the peak value. We do not find significant correlation between $r_{is,\,is}$ and $n_{is1,is2}$ for the full database.

The number of atoms, $n_{is,b}$, involved in moving from an IS to a transition state may be calculated in similar fashion. One might expect a larger number of atoms to be involved in a rearrangement with a large net change in the system coordinates and therefore large $r_{is,b}$ and $s_{is,b}$. However, results from our database do not reveal a significant correlation between the number of atoms in the IS−barrier step and any of the distance indicators.

The U_{is} dependence of the average of $r_{is,b}$, $s_{is,b}$, and $n_{is,b}$ is shown in Figure 13. With decreasing U_{is}, escape from an IS to a barrier involves a longer RP as shown by the increase of $\langle r_{is,b}\rangle$ and $\langle s_{is,b}\rangle$. Furthermore, $\langle n_{is,b}\rangle$ decreases with decreasing U_{is}, indicating that longer RP involve fewer atoms on average. The variance in these quantities for each IS energy band is smaller than the mean and has a similar U_{is} dependence.

Analysis of the database of RP does not show the growing cooperativity that is often postulated[4,5] as essential to the unique

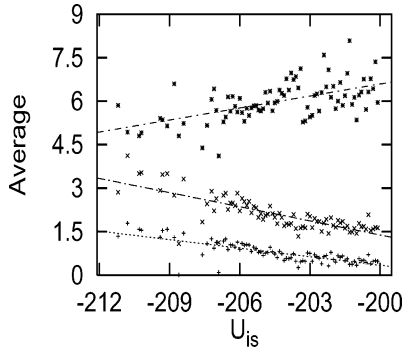

Figure 13. Inherent structure energy dependence of the mean value of, from bottom to top, $r_{is,b}$, $s_{is,b}$ (shifted by 1.0), and $n_{is,b}$ (shifted by 1.5). Also shown are the best fits to linear U_{is} dependence.

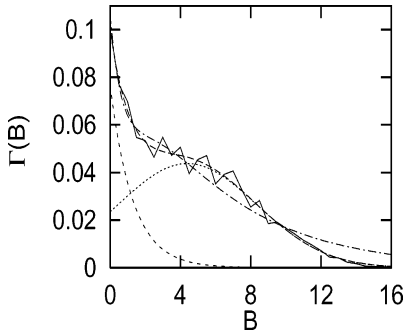

Figure 14. Distribution of barrier heights, B. The smooth curves are the least-squares fit to a sum of a Gaussian and an exponential, also shown individually for comparison, and the fit to the INM functional form (top curve at $B = 14$).

properties of supercooled liquids. Perhaps LJ is too simple, or perhaps the thermally sampled RP that enter true dynamics, as opposed to those taken unconditionally from the database, tell a different story.

B. Barriers. A key input for calculating rates is the barrier height, B, and its distribution, $\Gamma(B)$, shown in Figure 14. Some of the commonly used barrier height distributions in models for disordered system dynamics are the exponential, Gaussian, and uniform distributions,[19] none of which describe $\Gamma(B)$. It can be fit to a sum of an exponential and a Gaussian,

$$\Gamma(B) = 0.0766 \exp\left(\frac{-B}{1.31}\right) + 0.044 \exp\left(-\frac{1}{2}\frac{(B - 4.39817)^2}{3.94^2}\right) \quad (22)$$

Another functional form was used in a calculation based upon the INM density of states.[46] This form with the best fit parameters is $\Gamma(B) = 0.107 \exp(-0.182B) - 0.068071B \exp(-1.01B)$ and also gives a good representation, as show in Figure 14. Qualitatively similar distributions have also been found for polypeptides[47] using the INM approach, perhaps suggesting universal features of barrier height distribution in condensed systems.

The dependence of the barrier heights upon U_{is} is of considerable interest for determining the T dependence of relaxation. We have (Figure 15) obtained the conditional distribution, $\Gamma(B;U_{is})$, by binning the distributions for individual IS according to discrete U_{is} bands. An increase in barrier heights with decreasing IS energy is clearly revealed. In previous work[14] it was found that D is very well represented by the relation, $D = AT \exp(-1.16/T)$, where A is a constant. At the bottom of the landscape the distribution is peaked at $B \approx 8$, a value much greater than the activation energy of 1.16. On the top of the

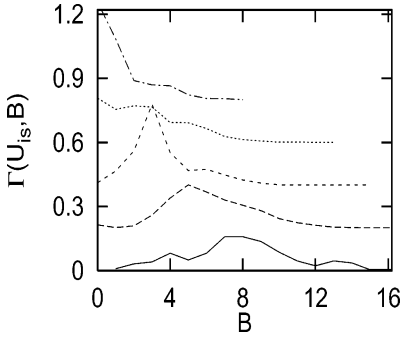

Figure 15. Inherent structure energy-dependent distribution of barrier heights $\Gamma(B;U_{is})$ for, bottom to top, $U_{is} = -212$, -210, -208, -206, and -204. The curves have been shifted by 0, 0.2, 0.4, 0.6, and 0.8 for clarity.

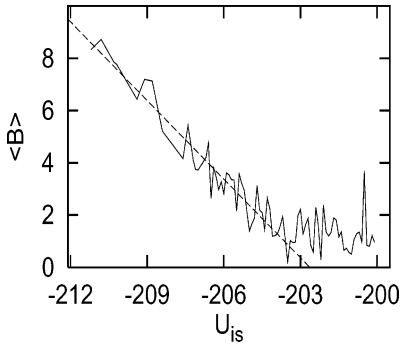

Figure 16. Average barrier height for escape from inherent structures with energy U_{is}. The smooth line is the fit of the data to $\langle B\rangle = -1.002U_{is} - 203.21$.

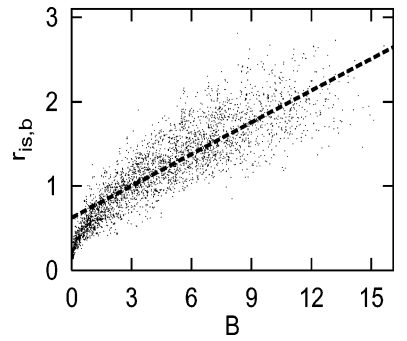

Figure 17. Dependence of IS−saddle distance in Cartesian space, $r_{is,b}$ on the barrier height, B. The straight line is a guide to the eye.

landscape the peak is at zero. These observations clearly illustrate the complexity of the relation between microscopic and macroscopic activation energies.

The U_{is} dependence of the average barrier height, $\langle B\rangle$, is shown in Figure 16. The overall dependence is linear for $U_{is} < -203$, above which there is no U_{is} dependence. The average barrier height increases with decreasing U_{is}, in agreement with findings of Grigera et al.[48] It has been suggested[16] that, for high T, the system moves among the higher order stationary points and the barriers are irrelevant; this would be facilitated by lower barriers at high U_{is}. It must be emphasized that the unconditional average is strongly influenced by the highest barriers, which might not be physically relevant.

Next we look at the correlations involving the barrier height. Because $r_{is,b}$ and $s_{is,b}$ are related, we consider the correlation of $r_{is,b}$ with B for the corresponding step along the RP. The data are presented as a scatter plot in Figure 17. Low B are associated with small $r_{is,b}$ and a linear dependence of $r_{is,b}$ on B can be seen. For larger B, more scatter indicates weaker correlation;

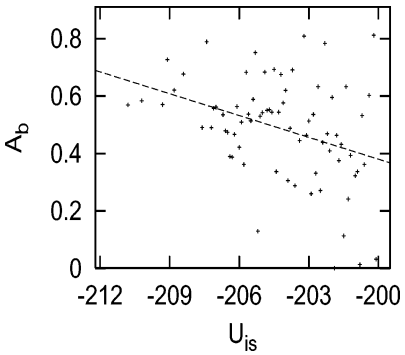

Figure 18. Dependence of the average value of the indicator for asymmetry in barrier heights, A_b, upon inherent structure energy, U_{is}.

however, the overall trend is that of a linear variation of $r_{is,b}$ with B. Larger barriers are therefore associated with a larger IS−barrier distance and longer rearrangement pathways. We do not find any correlation between B and $n_{is,b}$, which is unexpected because one usually assumes[4] a rearrangement involving a large number of atoms to involve a large barrier and *vice-versa*.

The soft potential, eq 21, has been used to model localized RP in the low-T thermodynamics of glasses. The parameter d_1 determines both the stress and the asymmetry. As it increases from zero the soft potential changes from a symmetric double well to an asymmetric double well to a single well. A good indicator for asymmetry is $A_b = (|B_{is1,b} - B_{is2,b}|)/B_{max}$, where B_{max} is the larger of the two barriers. We do not find a discernible correlation between A_b and either the transition state energy or U_{is} for the connected lower energy IS. For a given IS energy band there is a distribution of values of A_b and we consider the mean value as a function of saddle energy and the energy of the lower of the two connected IS. The U_{is} dependence is shown in Figure 18. The RP are on average quite asymmetric with A_b increasing down the landscape. Assuming asymmetry and stress are related, we conclude that the low-energy IS, sampled at low T, are stressed.

C. Analytic Methods. The soft potential can also be used to represent the RP. This form of $V(x)$ assumes for all soft modes a length scale of unity and an energy scale W. For convenience we select $W = 0.2$, on the basis of an estimate from fits in which W was optimized as a parameter. Fitting $V(x)$ to the triplets can be done in a number of ways. We minimize the squared difference in energies of the three stationary points and the corresponding energies from $V(x)$. Alternatively, one can fit the energies of the connected minima and the distance between them. The distribution of values for d_1 and d_2 are shown in Figure 19.

Buchenau and co-workers[28] obtained a distribution for the soft potential parameters that is independent of d_2. Zurcher and Keyes[29] used a step-function distribution of d_2, vanishing above an upper cutoff and constant below. Figure 19 shows a sharp falloff at large d_1 that could be approximated with a cutoff, but the low-d_1 distribution is not uniform and shows some structure, which could be a small-N effect. The coefficient d_1 is identified with frozen in stress and leads to asymmetry in the double well. Bucheneau's[28] proposed distribution is

$$p_1(d_1) = 0.231\left(\frac{T_g}{W}\right)^{3/4} \exp\left[-0.169\left(\frac{W}{T_g}\right)^{3/2} {d_1}^2\right] \qquad (23)$$

indicating that determining the variance of d_1, denoted θ^2, by simulation yields the glass transition temperature: $(T_g/W) = 0.485\theta^{4/3}$.

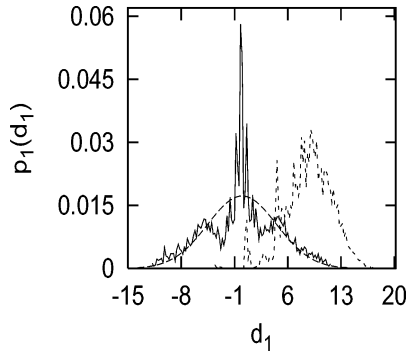

Figure 19. Distribution of d_1 (centered at zero) and d_2 obtained from fits of the soft potential to RP in the database. Also shown is a fit of the distribution of d_1 to a Gaussian.

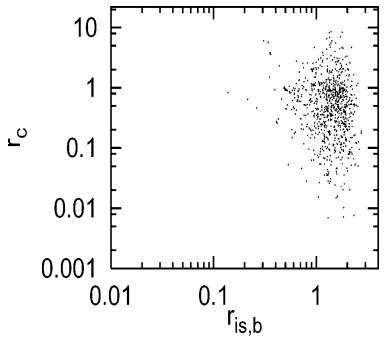

Figure 20. Cusp ratio, (r_c), for a quartic reaction path corresponding to the cusp catastrophe as a function of the path length. $r_c = 1$ corresponds to perfect agreement with the catastrophe theory prediction.

Fitting the entire range of d_1 gives $\theta^2 = 20.6481$ and $T_g = 0.6$. This value is too high, above the mode coupling temperature of 0.52 for this system. Zurcher and Keyes suggested that, in dynamic heterogeneity, slow and fast regions should possess high-d_1 and low-d_1, respectively. In a network fast regions dominate for parallel high connectivity, slow for serial one-dimensional connectivity. Fitting the central peak of the distribution, to capture the properties of the fast, unstressed regions, gives a variance of 0.33 and $T_g = 0.04$, which is close to the Kauzmann temperature for this system. Thus we have some evidence for parallel connectivity in LJ, and we confirm[3] that it is very nonfragile.

Though it is straightforward to identify the regions of parameter space that give the different types of soft potential wells, the dependence of functions upon their parameters may also be described with catastrophe theory. Starting with a symmetric double well, $-bx^4 + ax^2$, Wales[31] related the parameters to the characteristic features on the landscape, namely the barrier height, path length, and curvature at the saddle and obtaining the cusp ratio $r_c = 8B/(\omega r_{is,b}^2) = 1$. In Figure 20 we plot r_c as a function of $r_{is,b}$ for the smaller of the two barriers in a triplet. For small $r_{is,b}$ the cusp ratio is very close to 1 whereas a broader distribution is nonetheless centered at 1 for larger values of $r_{is,b}$. The expression for the cusp ratio was obtained using a symmetric double well that does not correspond to the actual RP, which are significantly asymmetric, as shown in Figure 18. This asymmetry reflects in deviations from $r_c = 1$. Our results provide additional confirmation of the applicability of catastrophe theory to the PEL.

V. Dynamics

With information about various features of the RP and their U_{is} dependence, the next step is relating them to macroscopic

dynamical quantities. The diffusion constant and its T dependence can be estimated from experiments or simulations. Some pertinent questions are: How is the diffusion constant related to the distribution of barrier heights, or the macroscopic activation energy to the microscopic barrier heights? Is transport dominated by activated processes involving barriers larger than T, or is it entropic in the sense that RP with $B \ll T$ exist, requiring no activation, and the meaningful "barrier" is the difficulty in finding them? What is the microscopic origin of the change in barrier heights with T?

The distributions $\Gamma(B;U_{is})$ and $P(U_{is},T)$ are important ingredients for a dynamical theory, but far from the whole story. Of course one must know the rate of crossing an individual barrier. For simplicity we will assume an Arrhenius dependence $R = R_0 \exp(-B/k_BT)$, although the appropriate limiting case of barrier-crossing theory for the PEL is unknown. Furthermore, information about the connectivity and correlations of the PEL is necessary to determine how the IS−transitions in a trajectory combine to yield the mean-square displacement, and D.

The *composite*[8,15,23,49,50] nature of the PEL is a crucial concept for dynamics. Except near the critical point, or possibly very close to the glass transition, correlations in liquids involve at most a few hundred particles. The "locality" of liquid-state problems must be included if the PEL approach is to be useful. This is done by recognizing that the $3N$-dimensional landscape is a composite of contributions of weakly interacting local spatial regions. The IS are built up from states of the regions. When a region changes its state, an IS−transition is recorded for the entire system. Because there are $z \sim O(1)$ particles in a region, their number is $N_r = N/z \sim O(N)$. The RP connected to a single IS represent rearrangements in different regions and are amenable to modeling based upon simple, few-particle ideas.

Consequently, as Stillinger and Weber[8] originally pointed out, the average total number of transitions per unit time, $\langle\omega_{is}\rangle$, is $\sim O(N)$, and the number of particles participating in a transition is $\sim O(1)$. The mean waiting time in an IS, $\langle t_{is}\rangle$, obeys $\langle t_{is}\rangle^{-1} = \langle\omega_{is}\rangle$, and thus $\langle t_{is}\rangle \sim O(1/N)$. Calculation of t_{is}, the mean for a given IS, from knowledge of the connected RP and barrier heights is a key piece of the puzzle. Relaxation of the entire system requires $\sim O(N)$ transitions. If, starting from a given IS, motion in the entire system is to be possible, the number of connected RP, denoted N_c, must be $\sim O(N)$. Thus a broad distribution of barrier heights could correspond to "slow" and "fast" spatial regions, as are indeed found[51] below T_c.

A. IS Waiting Times on the Composite Landscape. The functional form of the distribution of waiting times in the IS, $f(t)$, follows very generally from the composite property of the PEL. A region has a distribution of local waiting times, $f_{loc}(t)$, and at any instant a time will be assigned to all N_r regions, sampled from the distribution. The statement that the system makes a transition when any region makes a transition may be rephrased; the shortest local waiting time out of the N_r times is the waiting time of the system. Thus, as $N_r \to \infty$, $f(t)$ approaches[52] the Weibull distribution of minimal extremes,

$$f^W(t) = (\beta/\tau)(t/\tau)^{(\beta-1)}e^{-(t/\tau)^\beta} \tag{24}$$

where β is the "stretching exponent" and τ the characteristic time.

Previously[15] we obtained the $f(t)$ at several temperatures and fit the results, empirically, to a plain stretched exponential. Good fits were obtained with a T-independent $\beta = 0.50$. Despite an estimate that $N_r \approx 5$ for the $N = 32$ LJ system, the Weibull distribution is a better fit, with $\beta = 0.71$. Figure 21 demonstrates

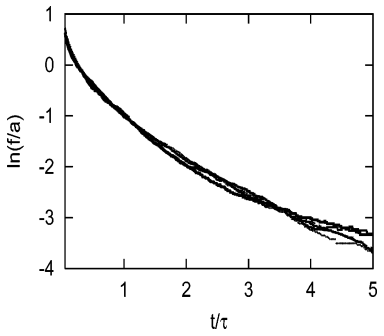

Figure 21. Log-normal master plot for the distribution of IS waiting times in unit-density LJ: Weibull distribution (smooth curve) with $\beta = 0.71$ and simulated distributions (overlapping points) for $T = 1.20$, 1.00, 0.80, 0.60, and 0.40 vs t/τ. Distributions are divided by multiplicative constant $a \equiv \beta/\tau$ (eq 24).

the goodness of the description with a master plot. Simulated data for $1.20 \geq T \geq 0.40$ all collapse on the Weibull function.

With the standard definition of the survival probability, $S(t) = \int_{-\infty}^{t} dt'\, f(t')$, the composite picture implies $S(t) = (S_{loc}(t))^{N_r}$. Differentiating and solving for f_{loc} yields

$$f_{loc}(t) = (\mathscr{R}(t)/N_r)S(t)^{1/N_r} \tag{25}$$

where $\mathscr{R}(t)$ is the usual expression for a time-dependent rate (not to be confused with the one-dimensional barrier crossing rate to be introduced in the next section), $\mathscr{R}(t) = f(t)/S(t)$. Equation 25 shows how a physically meaningful, intensive distribution of local waiting times may be calculated from composite quantities obtained from simulation.

The Weibull survival probability is the stretched exponential, $\exp(-(t/\tau)^\beta)$, the ubiquitous form taken by time correlations in supercooled liquids. Though the stretched exponential is usually derived as a superposition of exponential decays, an alternative is suggested by extreme value statistics. Suppose that a large number of molecules must cooperate for (e.g., rotational) relaxation to occur and that the entire group relaxes completely when the first member "attempts" to relax. The correlation function is then the survival probability for the minimal extreme, the stretched exponential.

B. Rates, Times, and Connectivity. Turning to the estimation of D, the PEL defines a $3N$-dimensional network of sites, the IS, connected by bonds, the RP. In network problems one can focus on sites or bonds. For a simple "bond" argument, consider the RP as resistors. The analogues are $D \leftrightarrow$ total conductivity, barrier crossing rate $\leftrightarrow$ bond conductivity, and inverse barrier crossing rate $\leftrightarrow$ bond resistance. With our simple assumption the "resistance" is a time, $\tau = \tau_0 \exp(B/k_BT)$; it is not a physical waiting time, because many RP lead out of an IS.

Textbook cases of a resistor network are parallel and serial connectivity. In the former, the total conductivity is proportional to the averaged bond conductivity, so $D \propto R(T) = R_0\langle\exp(-B/k_BT)\rangle$, where the average is over both barrier heights at a given U_{is}, and over U_{is} at a given T. Parallel connectivity is high connectivity, with many routes through the system, and those with the most high-conductivity bonds dominate D; when $\langle\exp(-B/k_BT)\rangle$ is evaluated, the Boltzmann factor favors the smallest barriers and highest rates.

In the serial case, the total conductivity is proportional to the inverse averaged bond resistance, $D \propto 1/\tau(T) = 1/(\tau_0\langle\exp(B/k_BT)\rangle)$. The paths through the system are literally one-dimensional and the highest barrier is rate-limiting; in $\langle\exp(+B/k_BT)\rangle$ the Boltzmann factor favors the highest barriers and slowest rates. The dominance of high barriers gives extremely

strong T dependence of D. With the number of RP connected to an IS $\sim O(N)$ on the composite landscape, "serial" is not, literally, possible. However, serial connectivity of local groups of IS could be related to the super-Arrhenius T dependence observed in fragile liquids.

For a more "site"-oriented, and more detailed approach, the IS−Markov approximation[14] is

$$D = \langle(\delta \boldsymbol{R}^2)\rangle\langle\omega_{is}\rangle/6N \tag{26}$$

where $\langle(\delta \boldsymbol{R}^2)\rangle$, the mean-square separation of successive IS in a trajectory, was found to be T-independent. With $\langle\omega_{is}\rangle \sim O(N)$ and $\langle(\delta \boldsymbol{R}^2)\rangle \sim O(1)$, it is seen that D is intensive.

To introduce individual barriers, let the distribution of waiting times in a single basin with IS energy U_{is} be exponential,

$$f(t) = R_{tot}e^{-tR_{tot}} \tag{27}$$

where $R_{tot} = \sum_i R_i$, the sum running over all the $N_c \sim O(N)$ barriers connected to the specific IS. The mean waiting time in the IS is then easily evaluated, $t_{is} = 1/R_{tot}$. In the thermodynamic limit, N, $N_c \rightarrow \infty$, the sum in R_{tot} will be self-averaging, and

$$t_{is} = 1/(N_c R(U_{is},T)) = \langle t_{is}(U_{is})\rangle \tag{28}$$

where

$$R(U_{is},T) = R_0 \int dB\, \Gamma(B,U_{is}) \exp(-B/k_BT) \tag{29}$$

Furthermore the thermodynamic $U_{is}(T)$ should dominate, and

$$\langle t_{is}\rangle = \langle\omega_{is}\rangle^{-1} = 1/(N_c R(U_{is}(T),T)) \tag{30}$$

with N_c regarded as a typical value. For a small system, not in the thermodynamic limit, the U_{is} fluctuations must be considered,

$$R(T) = \int dU_{is}\, P(U_{is},T)\, R(U_{is},T) \tag{31}$$

The IS−Markov approximation[14] becomes

$$D = \langle(\delta R^2)\rangle N_c R(T)/6N \tag{32}$$

It is completely consistent to have D proportional to the inverse mean waiting time in a multidimensional IS and also to the mean rate, $R(T)$, of crossing a one-dimensional barrier. Different arguments may be made for the serial case, where t_{is} does not contain a self-averaging sum, leading to $D \propto 1/\tau(T)$, a relation to the one-dimensional inverse time.

To illustrate the factors governing the T dependence of the averaged rate $R(T)$, we also calculate some other averages. First consider ignoring all U_{is} dependence and estimating an average, $R_1(T)$, from the unconditional distribution of barrier heights,

$$R_1(T) = R_0 \int dB\, \Gamma(B) \exp(-B/k_BT) \tag{33}$$

Another possibility is to correctly incorporate $P(U_{is},T)$ but to estimate the rate for each U_{is} band with its average barrier height,

$$R_2(T) = R_0 \int dU_{is}\, P(U_{is},T) \exp(-B(U_{is})/k_BT) \tag{34}$$

The cummulant expansion of $R_2(T)$ gives an average temperature-dependent barrier height, $B_{2C}(T)$,

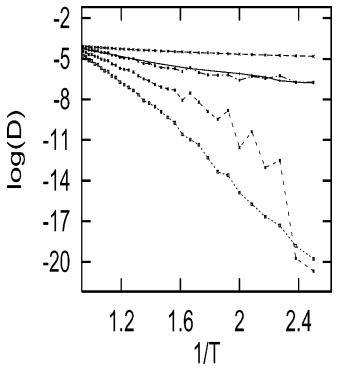

Figure 22. Natural log of, from top to bottom, $0.00142R_1(T)$, D and $0.0003R(t)$ (overlapping), $0.45R_2(T)$, and $1.4R_{2C}(T)$.

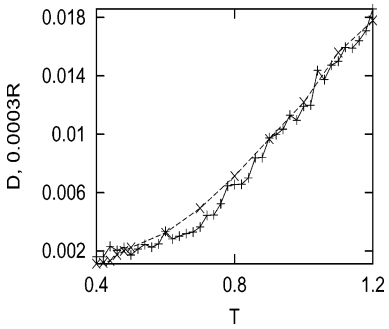

Figure 23. D (×, dashed line) and 0.0003 times one-dimensional rate, R (crosses and solid line) vs T.

$$B_2(T) = \int dU_{is}\, P(U_{is},T)\, B(U_{is}) \tag{35}$$

and we define $R_{2C}(T) = R_0 \exp(-B_{2C}(T)/k_BT)$.

C. Barriers and Diffusion. The various averaged rates and inverse times may now be evaluated and compared to D, Figure 22. The most important observation is that the "true" average, $R(T)$, captures the T dependence of D amazingly well. An expanded view is in Figure 23. This suggests parallel connectivity, which may be generally true or, possibly, a property of a nonfragile liquid lacking super-Arrhenius behavior.

The behavior of the other averages shows that the detailed treatment of the PEL is essential to the good agreement. All things being equal, the parallel average will favor the lowest barriers. The rate ignoring the U_{is} dependence of the barrier heights, R_1, has a very weak T dependence because it is dominated by the very low barriers prevalent (Figure 15) at high U_{is}. By contrast, employing a U_{is}-dependent average barrier height gives a rate, R_2, that is dominated by the high barriers; *any* unweighted average of barrier heights will have this property. Because, furthermore, the average barrier increases with decreasing U_{is}, too-strong, super-Arrhenius T dependence results that is particularly poor for low T. The error is somewhat mitigated in the cummulant expansion. The effective barrier $B_2(T)$, eq 35, gets contributions from the low barriers at high U_{is} even at low T, and so is smaller than the effective barrier for R_2. Nonetheless, the high barriers are still overweighted and the T dependence too strong.

In every case, corresponding definitions for $\tau(T)$, which naturally favor high barriers, lead to a stronger T dependence. No inverse *one-dimensional* time represents D, again causing no contradiction with $D \propto t_{is}^{-1}$. Diffusion for this system is proportional to the averaged single-RP rate, corresponding to high, parallel connectivity.

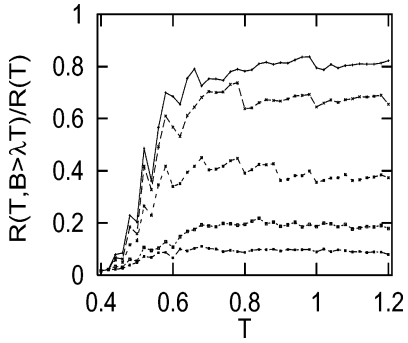

Figure 24. Ratio $R(T,B>\lambda T)/R(T)$ describing the relative contribution to the rate from barriers larger than λT (LJ units) at different T. Top to bottom, $\lambda = 0.3$, 0.5, 1.0, 2.0, and 3.0.

Because the averaged rate has the same T dependence as D, it has the same macroscopic activation energy. The value mentioned earlier, 1.16, comes from fitting D/T. A fit to D gives $E_A = 1.8$; a factor of T is significant when only a small range of D is available. The barriers contributing to R, appropriately weighted, may be seen from the distributions in Figure 15. There is no distinctive feature at $B = 1.16$ or 1.8. The barrier distribution shifts strongly to higher B with decreasing U_{is}, which is decreasing T, but no super-Arrhenius behavior results. This indicates that the Boltzmann factor e^{-B/k_BT} is steering the system away from the high barriers. The situation would be radically different with serial connectivity. It may be that the increasing barrier heights are required to even attain a T dependence as strong as Arrhenius. In sum, at least for LJ, the relation between the microscopic barriers and the macroscopic activation energy is complex. Perhaps some other systems have dominant microscopic barriers that directly determine E_A.

D. Activated vs Entropic transport. In an activated transport scenario, diffusion occurs via barriers with $B \gg k_BT$. On the other hand for entropic transport, the system needs to find a pathway with $B \ll k_BT$, and their availability is crucial. The results of the last section—increasing barriers but constant E_A—seem to indicate that the mechanism in the LJ system is entropic. To explicitly explore the contribution of low- and high-energy barriers to D, we split the B integral for the rate $R(T)$ into two parts, the contributions from all barriers less than λT, $R(T,B<\lambda T)$, and the remainder, $R(T,B>\lambda T)$. LJ units will be used in the detailed calculations. By varying λ, a good picture of the contribution of barriers with different heights with respect to T can be obtained; we select $\lambda = 0.3$, 0.5, 1.0, 2.0, 3.0.

Shown in Figure 24 is the ratio, $R(T,B>\lambda T)/R(t)$, the fractional contribution to the rate from barriers larger than λT. For $B > 3.0\ T$, which could be representative of activated processes, the ratio is 0.1 for $T \gtrsim 0.7$, indicating that transport is not activated by this definition. For lower T, the contribution of barriers greater than $3T$ decreases and reaches an almost constant small value of $\approx$0.03. Thus at low T, when the system is near the bottom of the PEL where barriers are higher, diffusion comes from *low* barriers.

As λ decreases 10-fold from 3.0 to 0.3, the contribution of $B > \lambda T$ for $T \gtrsim 0.7$ increases from 0.1 to 0.8. The rate gets a significant contribution from $B > 0.3T$, but of course this need not be activated. For low temperatures the contribution from barriers larger than $0.3T$ falls once more to a small value $\approx$0.03. Thus, e.g, at $T = 0.4$ the rate is dominated by barriers smaller than 0.12, which are the lowest available to the system. Activation should not be necessary for crossing such barriers; the system just needs to find them. This is a clear demonstration of entropic transport at low T. The mechanism of diffusion at high T is a combination of activated and entropic transport. One might speculate that the dominance of the entropic mechanism begins at T_c.

VI. Discussion

By current standards, $N = 32$ is a very small system. However, with 10 000 minima and 18 000 transition states, it is complex compared to simple phenomenological models, and so we call it a model. Furthermore, given that the PEL is a composite, the clearest picture of IS dynamics is obtained when the system exceeds the size of a local region by only what is necessary to mitigate finite-size effects. A further increase in size yields a superposition of independent events that serves only to make the extraction of physically meaningful local information difficult.

Computationally tractable power series methods were demonstrated, which yield the harmonic and anharmonic vibrational free energy. Because they employ a fit to the fluctuating quantity $U(U_{is},T) - U$, they can claim no credit for reproducing simulated $U_{is}(T)$, even though the harmonic approximation cannot do so. The point is that other thermodynamic properties, in particular the entropy, may then be calculated. Obtaining S_c by subtracting the vibrational entropy from $S(T)$, the Adam−Gibbs relation[4] is verified.

A survey of the characteristic features of a RP indicates proportionality between the IS−saddle Cartesian and contour distances, $r_{is,b}$ and $s_{is,b}$, and between those distances and the barrier height B. There is no apparent correlation between the curvature at the saddle and the barrier height, suggesting caution in interpreting one-dimensional models in which such a relation is implicit. A connection to real space features of a rearrangement can be made via the number of atoms involved in the rearrangement. Though one might expect[4] a low-energy barrier to be associated with fewer rearranging atoms, this trend is also not supported by our database.

The distribution of the number of atoms involved in an IS transition, with no thermal weighting, is peaked at $n_{is1,is2} \approx 9$. Previously,[15] we found that the average number of atoms participating in the actual transitions was 6.61 for $1.2 \geq T \geq 0.4$. A fit of the random energy model[23] expression for the DOS to simulation gave the number of atoms in a local region as 7.0; this quantity should be roughly equivalent to $n_{is1,is2}$. Thus three independent estimates confirm that about seven atoms move in the diffusive rearrangements of this system.

The U_{is}-dependent distribution of barrier heights, $\Gamma(B;U_{is})$, is a crucial quantity for describing the process of escaping from an IS. Still, much more is required for a complete theory of IS dynamics, including a detailed barrier-crossing theory and more global information about the arrangement of the IS (connectivity). Our primary dynamical results are (1) the averaged T-dependent rate, calculated with a crude Boltzmann-factor anzatz for individual barier crossing rates, very closely tracks $D(T)$, and (2) barriers with $B < k_BT$ dominate the calculation − entropic transport − especially at the lowest T. The former is our expectation for parallel conductivity. The latter is not really surprising, even though the barriers are clearly increasing toward the bottom of the PEL, because it is the long-discussed entropic scenario. It may support the conjecture of Kivelson et al.[53] that low- or zero-barrier "equipotential ribbons" are important in supercooled dynamics.

By contrast, a recent paper[54] on a small-N simulation of the binary LJ mixture concludes that activated barrier crossing is dominant. It seems worth mentioning that our work on LJ differs from that of Heuer and co-workers on the LJ mixture on several

points. (1) We found[14] that IS dynamics was approximately a random walk below T_c and were able to *quantitatively* evaluate D with the Markov approximation, eq 26. They argued[55] that the process among the IS was strongly nonrandom, and that the introduction of metabasins was necessary. (2) We find that the distribution of waiting times in the IS obey a Weibull distribution (or[15] a stretched exponential). They find[55] an inverse power law decay. (3) As just mentioned, we differ on entropic vs activated transport. Of course, because they believe that metabasins are essential, their activation barrier is one between metabasins, and this can be much larger than the barrier between IS. It will be very interesting to see if these differences are properties of nonfragile (LJ) vs fragile (binary LJ mixture) liquids, or something else.

Acknowledgment. We thank Frank Stillinger, Francesco Sciortino, Emilia La Nave, and Joohyun Kim for valuable discussions. This work was supported by NSF Grant CHE-0090975.

References and Notes

(1) Angell, C. A. Formation of Glasses from Liquids and Biopolymers. *Science* **1995**, *267*, 1924. Debenedetti, P.; Stillinger, F. H. Supercooled Liquids and the Glass Transition. *Nature* **2001**, *410*, 259.
(2) Goetze, W.; Sjogren, L. *Rep. Prog. Phys.* **1992**, *55*, 241.
(3) Ferrer, M.; Kivelson, D. *J. Chem. Phys.* **1999**, *110*, 10963.
(4) Adam, G.; Gibbs, J. H. *J. Chem. Phys.* **1965**, *43*, 139.
(5) Kivelson, D.; Tarjus, G. *J. Chem. Phys.* **1998**, *109*, 5481.
(6) Goldstein, M. *J. Chem. Phys.* **1969**, *51*, 3728.
(7) Stillinger, F. H. *Science* **1995**, *267*, 1935.
(8) Stillinger, F. H.; Weber, T. A. *Phys. Rev. A* **1983**, *28*, 2408; *Science* **1984**, *225*, 983.
(9) Stillinger, F. H.; Weber, T. A. *J. Chem. Phys.* **1984**, *81*, 5095.
(10) Debenedetti, P. G.; Stillinger, F. H.; Truskett, T. M.; Roberts, C. J. *J. Chem. Phys B* **1999**, *103*, 7390.
(11) La Nava, E.; Mossa, S.; Sciortino, F. *Phys. Rev. Lett.* **2002**, *88*, 225701. Shell, M. S.; Debenedetti, P. G.; La Nave, E.; Sciortino, F. *J. Chem. Phys.* **2003**, *118*, 8821.
(12) Speedy, R. *J. Phys. Condens. Matter* **2003**, *15*, S1243.
(13) Keyes, T.; Chowdhary, J. *Phys. Rev. E* **2004**, *69*, 041104.
(14) Keyes, T.; Chowdhary, J. *Phys. Rev. E* **2001**, *64*, 032201.
(15) Keyes, T.; Chowdhary, J. *Phys. Rev. E* **2002**, 65, 041106.
(16) Angelani, L.; Di Leonardo, R.; Ruocco, G.; Scala, A.; Sciortino, F. *Phys. Rev. Lett.* **2000**, *85*, 5356. Cavagna, A. *Europhys Lett.* **2001**, *53*, 490.
(17) Stillinger, F. H. *Phys. Rev. E* **1999**, *59*, 48.
(18) Monthus, C.; Bouchaud, J. P. *J. Phys. A* **1996**, *29*, 3847.
(19) Argyrakis, P.; Milchev, A.; Pereyra, V.; Kehr, K. W. *Phys. Rev. B* **1995**, *52*, 3623.
(20) Limoge, Y.; Bocquet, J. L. *Phys. Rev. Lett.* **1990**, *65*, 60.
(21) Mussawisage, K.; Wichmann, T.; Kehr, K. W. *J. Phys. Condens. Matter* **1997**, *9*, 1181.
(22) Bryngelson, J.; Wolynes, P. G. *J. Phys. Chem.* **1989**, *93*, 6902.
(23) Madan, B.; Keyes, T. *J. Chem. Phys.* **1993**, *98*, 3342. Keyes, T. *Phys. Rev. E* **2000**, *62*, 7905. Keyes, T.; Chowdhary, J.; Kim, J. *Phys. Rev. E* **2002**, *66* 051110.
(24) Wales, D. J. *J. Chem. Phys.* **1994**, *101*, 3750.
(25) Doye, J. P. K.; Wales, D. J. *J. Chem. Phys.* **1995**, *102*, 9659.
(26) Miller, M. A.; Doye, J. P. K.; Wales, D. J. *Phys. Rev. E* **1999**, *60*, 3701.
(27) Angelani, L.; Parisi, G.; Ruocco, G.; Viliani, G. *Phys. Rev. Lett.* **1998**, *81*, 4648.
(28) Buchenau, U. *J. Mol. Structure* **1993**, *296*, 275. Gil, L.; Ramos, M. A.; Bringer, A.; Buchenau, U. *Phys. Rev. Lett.* **1993**, *70*, 182.
(29) Zurcher, U.; Keyes, T. *Phys. Rev. E* **1977**, *55*, 6917.
(30) Gilmore, R. *Catastrophe Theory for Scientists and Engineers*; Wiley: New York, 1981.
(31) Wales, D. J. *Science* **2001**, *293*, 2067.
(32) Press, W. H.; Teukolsky, S. A.; Vetterling, W. T.; Flannery, B. P. *Numerical Recipies in C*, 2nd ed.; Cambridge University Press: London, 1992.
(33) Sciortino, F.; Kob, W.; Tartaglia, P. *Phys. Rev. Lett.* **1999**, *83*, 3214.
(34) Sastry, S. *J. Phys.: Condens. Mattter* **2000**, *12*, 6515.
(35) Mossa, S.; La Nava, E.; Stanley, H. E.; Donati, C.; Sciortino, F.; Tartaglia, P. *Phys. Rev. E* **2002**, *65*, 041205.
(36) Scala, A.; Starr, F. W.; La Nave, E.; Sciortino, F.; Stanley, H. E. **2000**, *406*, 166.
(37) Choquard, P. F. *The Anharmonic Crystal*; Benjamin, New York, 1967.
(38) Calvo, F.; Doye, J. P. K.; Wales, D. J. *J. Chem. Phys.* **2001**, *115*, 9627.
(39) Lacks, D. J.; Shukla, R. C. *Phys. Rev. B* **1996**, *54*, 3266.
(40) Sastry, S.; Debenedetti, P. G.; Stillinger, F. H. *Nature* **1998**, *393*, 554.
(41) Johari, G. P. *J. Chem. Phys.* **2000**, *113*, 751.
(42) Sastry, S. *Nature* **2001**, *409*, 164.
(43) Li, W.-X.; Keyes, T.; Sciortino, F. *J. Chem. Phys.* **1998**, *108*, 252.
(44) Keyes, T. *J. Chem. Phys.* **1994**, *101*, 5081. Keyes, T. *J. Phys. Chem.* **1997**, *101*, 2921.
(45) Middleton, T. F.; Wales, D. J. *Phys. Rev. B* **2001**, *64*, 024205.
(46) Keyes, T. *J. Chem. Phys.* **1994**, *101*, 5081.
(47) Straub, J. E.; Thirumalai, D. *Proc. Natl. Acad. Sci., U.S.A.* **1993**, *90*, 809.
(48) Grigera, T. S.; Cavagna, A.; Giardina, I.; Parisi, G. *Phys. Rev. Lett.* **2002**, *88*, 055502.
(49) Madan, B.; Keyes, T. *J. Chem. Phys.* **1993**, *98*, 3342.
(50) Xia, X.; Wolynes, P. G. *Proc. Natl. Acad. Sci.* **2000**, *97*, 2990; *J. Phys. Chem. B* **2001**, *105*, 6570; *Phys. Rev. Lett.* **2001**, *86*, 5526.
(51) Ediger, M. *Annu. Rev. Phys. Chem.* **2000**, 51.
(52) Coles, S. *An Introduction to Statistical Modeling of Extreme Values*; Springer: Berlin, 2001.
(53) Kivelson, D.; Tarjus, G. *J. Phys. Chem. B* **2001**, *105*, 11854.
(54) Doliwa, B.; Heuer, A. *Phys. Rev. E* **2003**, *67*, 031506.
(55) Doliwa, B.; Heuer, A. *Phys. Rev. E* **2003**, *67*, 030501(R).